Experimental observation of the number of visible defects produced in individual primary damage cascades in irradiated tungsten

D.R. Mason[1] , X. Yi[2] , A.E. Sand[3] , S.L. Dudarev[1]

[1] *CCFE, UK Atomic Energy Authority, Culham Science Centre, Abingdon, Oxfordshire OX14 3DB, United Kingdom*
[2] *School of Materials Science and Engineering, University of Science and Technology Beijing, 100083, Beijing, China*
[3] *Department of Physics, University of Helsinki, P.O. Box 43, FI-00014, Helsinki, Finland*

PACS 61.72.J- – Point defects and defect clusters
PACS 61.80.Az – Theory and models of radiation effects
PACS 68.37.Lp – Transmission electron microscopy (TEM)

Abstract – We present a new analysis of nanoscale lattice defects observed after low-dose *in situ* self-ion irradiation of tungsten foils at cryogenic temperature. For decades, defect counts and size-frequency histograms have been the standard form of presenting a quantitative analysis of the nanoscale "black-dot" damage typical of such irradiations. Here we demonstrate a new statistical technique for generating a probability distribution for the number of defects produced in a single cascade. We show that while an average of fewer than one defect is observed per incident ion, the number of cascades with two or more visible defects produced is significant.

Introduction. – *In situ* irradiation of TEM-transparent foils offers great control over damage production and thermal history, and becomes a very valuable tool for nuclear materials research when we can extract data comparable to our simulations of physical radiation damage processes. For decades, quantitative analyses of irradiation damage in the form of nanoscale defects as been presented as defect counts and size-frequency histograms [1–3], but the position correlation of the defects has been under-utilised, due to the time-consuming nature of identifying a sufficient number of spots by eye to make such an analysis practical. The importance of this data, present in micrographs but unexploited, has recently become clearer. Primary damage cascades are inherently random processes, and their subsequent microstructural evolution may well be dominated by rare events [4–7]: the evolution of point defects and small clusters will be strongly skewed if a large dislocation loop is also generated during the heat spike phase [8], and if multiple large loops are in close proximity then their elastic interaction can lead to self-trapping [9].

Recently we have developed techniques [10, 11] for automating the analysis of black-dot damage, which produces a reproducible list of spot positions and sizes in a few minutes. We have been able to verify that primary damage cascade events in ultra-high purity tungsten foil produce a power-law size-frequency distribution of defects [10], and have accounted for observed deviations from power-law behaviour due to subcascade branching [12]. We have also been able to show, from analysis of the pairwise radial distribution function, that the characteristic size of individual cascades is of order one nanometer [11]. In this letter we perform a new type of analysis, to find the number of visible defects produced in a single cascade.

***In situ* TEM experiments.** – Experimental data for the count of visible defects per cascade is generated from *in situ* self-ion irradiations of high purity tungsten foils, performed at cryogenic temperature at the IVEM-Tandem Facility at Argonne National Laboratory. Further information about these experiments can be found in ref [11]. This paper contains a novel analysis of the same set of micrographs. It is known that the collapse of displacement cascades in self-ion irradiated tungsten produces large, nanometre-scaled (and therefore TEM visible) dislocation loops [9, 10]. We perform experiments at cryogenic temperature (30K), where the mobility of irradiation-induced defects is reduced, though we acknowledge that Brownian motion of defects due to quantum fluctuations of atomic positions associated with their zero

point motion will still be present [13] and so loop loss to the surface can still occur.

3mm discs were cut from ultra-high purity tungsten sheets (supplied by Plansee with typical > 99.996 wt% purity). These were then heat-treated in vacuum at 1673 K for 20 hours, before being electropolished to electron transparency thickness ($\lesssim$100nm). See refs [9, 14] for full technical details of the sample prepation. The samples were irradiated *in situ*, at an incidence angle 15° off normal, up to a fluence of $1.25 \times 10^{16} \mathrm{W}^{+}/\mathrm{m}^{2}$.

(001) grains were selected for analysis, imaged in weak-beam dark-field conditions, using (**g** =200, 4.25g; **g** =200, 4.75g; **g** =200, 5.25g; **g** =110, 5.25g; **g** =110, 7.25g; and **g** =110, 7.75g). Regions were superimposed using the convergent weak beam technique [15], and analysed using the automated technique described in [10,11]. We present results for incident ion energies 50keV, 150keV and 400keV. A typical micrograph, together with a computer-generated analysis of the defect positions, is shown in figure 1. A quick (Kinchin-Pease) SRIM calculation [16] with threshold displacement energy $E_d = 55.3$eV [9], gives an average 0.006dpa in the damage region for 50keV ions rising to 0.01dpa for 400keV ions. A summary of the irradiation analyses is presented in table 2.

An important part of this analysis is the use of meaningful errorbars. The automated procedure for identifying spots fits a 2-d Gaussian profile to each potential spot, so for each spot we can construct the t-statistic

$$t^{\star} = \frac{\bar{I} - I_0}{\sigma_I / \sqrt{n}} \tag{1}$$

where $\bar{I}$ is the average intensity within one standard deviation of the maximum, a region covering n pixels. The background has average intensity I_0 and standard deviation σ_I. $t^{\star}$ is high for larger, or brighter spots, so we can use this to select or reject faint spots. However it is not correct to assume $t^{\star}$ follows the t-distribution with $n-1$ degrees of freedom, as bright regions-of-interest are preselected [11]. Instead we can run our spot detection program on *unirradiated* samples, prepared at the same time and in the same manner as the irradiated samples. This gives the number of erroneously identified 'spots' as a function of a critical $t^{\star}$ value. This gives us a probability for a type-I error (false positive), which we can read as a significance level for identifying a spot as a radiation-induced defect. The significance level as a function of the threshold value of $t^{\star}$ for the input parameters used is given in table 1. We report results with widely varying significance levels because of the difficulty in correctly accounting for type-II errors (false negative), where a spot is ignored for being too faint.

Size-frequency histograms are presented in figure 2. Note that the average number of visible defects per cascade is order 0.1-0.3, indicating that most cascades do not produce any visible defects. We observe that smaller- and therefore also fainter- spots are more difficult to confidently identify on the micrograph, a conclusion also reached recently by Liu et al [17]. Figure 2 makes it plain that the 'count' and 'average' diameter of defects are both functions of the intensity threshold used. We suggest that the use of a single figure metric to characterize primary damage may be misleading, due to false-positive or false-negative identification errors for the smallest, faintest defects. As an indication of this problem, we can compare the total count of visible defect clusters per cascade computed here (with a baseline for significance determined by unirradiated micrographs), with an earlier analysis of the same micrographs (with a baseline for significance based on random noise), ref [11]. At 50 keV, our new confidence interval is [0.06 : 0.22] defect clusters per ion, previously we had a single figure 0.134. At 150 keV the interval and previous values are [0.08 : 0.21] and 0.163, and at 400 keV [0.16 : 0.27] and 0.288. The 400 keV implantation confidence interval does not contain the previous result, which we attribute to over-counting the smallest, faintest spots in the earlier work. There is no significant difference in the spatial correlation results if the data sets are interchanged, as expected if the error was from false-positive results. A single count or size of defects may be more relevant for a more evolved microstructure, where Ostwald ripening may remove the smallest defects.

Analysis. It is important to note that while many radiation-induced defects can be counted, appearing on the micrographs as spots [18], their proximity alone is insufficient to confidently state that a pair originates from a single cascade. A statistical method is required to find the most likely distribution function for the number of visible defect clusters per cascade event. In our previous paper, ref [11], we found a peak in the pairwise radial distribution function for spot placement, and concluded that multiple visible defect clusters must be formed in a single cascade event, but were unable to prove how many. In this paper we use higher order spatial correlation functions to find the answer.

We want to compute the probability of a cascade generating exactly m spots on the micrograph, which we denote $P_{\mathrm{clust}}(m)$. Start by considering the probability of counting k spots in an observed area A. This probability must be the sum over all possible combinations of having a number k_1 one-spot cascades, k_2 two-spot cascades and so on.

$$P_{\mathrm{total}}(k; A) = \sum_{k_1, k_2, \ldots} \delta_{k_1 + 2k_2 + \ldots, k}\, p(k_1, k_2, \ldots; A), \tag{2}$$

where $p(k_1, k_2, ...; A)$ is the probability of finding k_1 cascades each containing one visible defect, k_2 cascades each containing two visible defects, etc., in area A. We now make the assumption that cascade overlap may be neglected (see ref [14] for a detailed justification). Each cascade is therefore assumed independent, and we can write

$$p(k_1, k_2, \ldots; A) = p(k_1; A) p(k_2; A) \ldots . \tag{3}$$

$p(k_m; A)$ is the probability distribution of observing k_m m-spot cascades in an area A. This probability is expected to

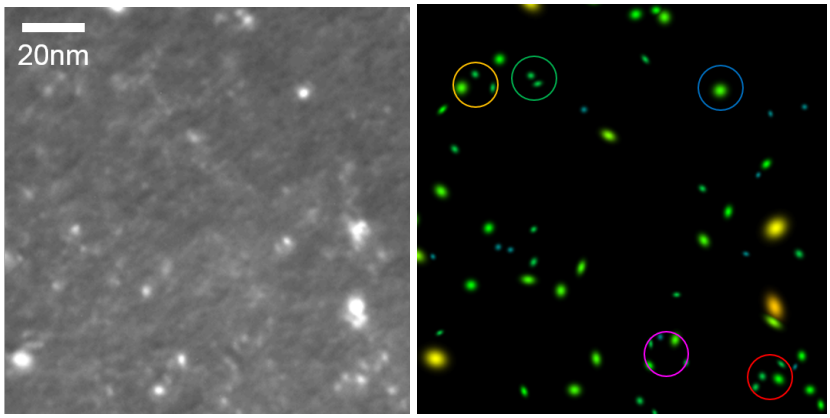

Fig. 1: Left: TEM micrograph of *in situ* irradiation of 150keV self-ion irradiation of UHP tungsten foil at 30K. WBDF imaging shown with highly exaggerated contrast. Right: Analysis of the position and size of defect clusters. Spot colours denote defect cluster diameter. Circles of diameter 14nm are also indicated, containing one to five spots (circle colours blue, green, yellow, red, pink). But the proximity of spots alone can not be used to determine if they originated in one cascade. Our analysis proceeds by finding all the minimum enclosing circles containing m spots, and fitting the distribution. More micrographs showing the dependence on $t^\star$ are added in the supplementary material.

$t^\star$	α
3.1	0.15
6.3	0.025
12.7	0.001

Table 1: Critical values of $t^\star$ used to find a significance level α, with the settings used for the analysis of these images. A significance value α is the probability a type-I error - the natural background variation being (erroneously) identified as a spot.

	Ion energy (keV)		
	50	150	400
regions studied	4	8	8
total area (nm^2)	1.71e+07	2.96e+07	3.05e+07
incident ions	21300	37000	36100
visible clusters per cascade	0.15 [0.06:0.22]	0.14 [0.08:0.21]	0.21 [0.16:0.27]
ion depth (nm)	6.9	13.7	30.6
inter-cascade length (nm)	8.2	10.5	13.4

Table 2: Results for the analysis of primary cascades in TEM micrographs. The depth of the damage region L is computed using SRIM [16]. The number of visible clusters per cascade has three values- we report the significance level $\alpha = 0.025$, with the bracketed region the interval $[\alpha = 0.001, \alpha = 0.15]$. The characteristic average inter-cascade length is discussed in the text. Comprehensive size-frequency histogram data is provided in supplementary material.

be Poisson distributed as their generation is independent. The average count of m-spot cascades in an area A is $\lambda_m = \rho A P_{\mathrm{clust}}(m)$, where ρ is the irradiation density (incident ions per unit area).

$$p(k_m; A) = \mathrm{Po}_{\lambda_m}(k_m) \equiv \frac{(\lambda_m)^{k_m}}{k_m!} \exp(-\lambda_m). \qquad (4)$$

As noted above, we can not directly identify two-spot cascades. But we *can* count the number of pairs of spots in an area A. The expected number of pairs of spots in area A is $\langle n_{pair}(A)\rangle = {}^1\!/_2 \sum_k k(k-1) P_{\mathrm{total}}(k; A)$. Similarly the expected number of m-tuples of spots in area A is a sum over all possible combinations of m spots:

$$\begin{aligned} \langle n(m; A)\rangle &= \sum_k \frac{k!}{m!(k-m)!} P_{\mathrm{total}}(k; A) \\ &= \sum_k \sum_{k_1,k_2,\ldots} \frac{k!}{m!(k-m)!} \delta_{k_1+2k_2+\ldots,k} \\ &\quad \times \mathrm{Po}_{\lambda_1}(k_1)\mathrm{Po}_{\lambda_2}(k_2)\ldots \end{aligned} \qquad (5)$$

This can be measured from the micrographs as follows. For each spot in the micrograph we find each possible set of m spots which includes it. We construct the minimum enclosing circle (MEC) around the set, defined to enclose the centres of the spots as determined by analysis of the

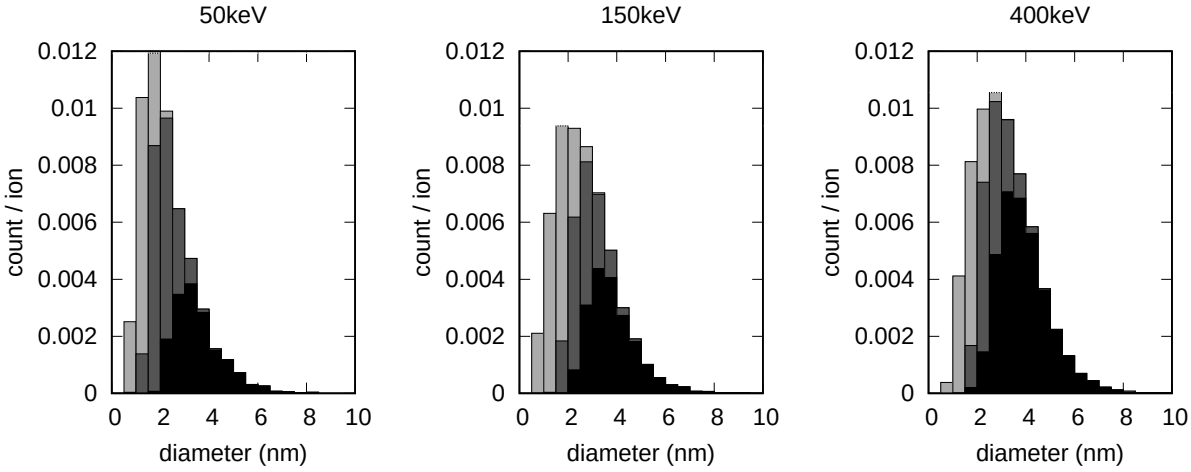

Fig. 2: The experimentally observed size-frequency histogram for the three ion implantation energies considered. The shading indicates the count of spots with intensities over significance levels $\alpha = 0.001$ (black), through 0.025 (mid-grey) to 0.15 (light grey). Presenting the data in this manner makes it clear that smaller, and therefore fainter spots are more difficult to confidently identify as radiation-induced damage on the micrograph.

micrograph. Write $N(m;A)$ as the number of minimum enclosing circles containing at least m spots with area less than or equal to A. Note that $N(1,A) = N(1,0)$ is the total count of spots in the micrograph. We can then best fit $P_{\text{clust}}(m)$ to match the (theoretical) $\langle n(m;A)\rangle$ to (experimental) $N(m;A)$, normalised to reproduce the total count of spots.

We must choose a characteristic area A. To do this, note that we can compute a typical inter-cascade length assuming uniform cascade generation within a penetration depth computed using SRIM [16], combined with the ion fluence 1.25×10^{16} $\text{W}^{+}\text{m}^{-2}$, and present the results in table 2. This characteristic length, taken as the cube-root of the average volume per cascade, can be compared with the typical separation between visible clusters (3-4 nm [11]), and the size of the enclosing circles used in our analysis. We present the results for $N(m;A)$ in figure 3 using minimum enclosing circles with diameter less than or equal to $d = 8nm$. As the typical inter-cascade length is greater than 8nm, we conclude that the count of spots in each enclosing circle is not dominated by multiple cascades, and that our experiments are not dominated by cascade overlap. The results are in fact insensitive to enclosing circle diameter between $d = 8nm$ and $d = 16nm$. The $t^{\star}$ thresholds for the identification of smaller, fainter spots give error bars for this calculation. The lower threshold we consider ($\alpha = 0.15$) gives the most spots. This level also gives the upper limit of the number visible spots m per MEC. This proves that the faintest spots we are recording are clustered, and so suggests that this low threshold is capturing faint defect clusters produced in cascades.

We present fits for the number of defect clusters produced per cascade, $P_{\text{clust}}(m)$ in figure 4.

Without any prior assumptions, except for no cascade overlap, we find that while very few cascades produce visible defect clusters, we can still find a fit for $m = 0, 1, 2, 3$ visible defects per cascade. We find no requirement for $m \geq 4$ defects per cascade, though this may be because such events are very rare, and we have insufficient data.

Discussion and Conclusions. – In this work we have made no attempt to identify the Burgers vectors or character of the defect clusters, only to count the visible defect clusters. Vacancy clusters and voids would be too faint to see in these imaging conditions [18], so we would expect visible objects of the size seen in these micrographs to be interstitial- or vacancy- type loops as these are the known low-energy structures [19, 20].

An interesting question to ask is whether the distribution $P_{\text{clust}}(m)$ itself fits a simple analytical form. The simplest possible model to propose is that $P_{\text{clust}}(m)$ is Poisson distributed. This would suggest that large visible defects are produced independently of each other within a cascade. We could argue that the kinetic energy of the incident ion is nearly all lost to phonons, with only a small fraction remaining as the excess potential energy of the residual lattice defects, so the Poisson process is within energy space. The difficulty with this model is that any subsequent evolution of the microstructure, be it loss of clusters to the surface or aggregation/recombination of defects would bring the observed distribution away from Poisson. Recent theoretical and experimental observations [9, 11, 12], suggest a dominant mechanism for loop retention in a thin foil irradiation experiment like this one is mutual elastic self-trapping. Put simply, if only one large loop is generated in a cascade, there is little to prevent it being attracted to the surface and lost [21, 22]; if two or more are generated they can mutually self-trap [23]. We might therefore expect to see fewer single-spot-cascades than were actually generated. Fitting $P_{\text{clust}}(m) = \text{Po}_f(m)$ for a single value f to the observed count of m-tuples

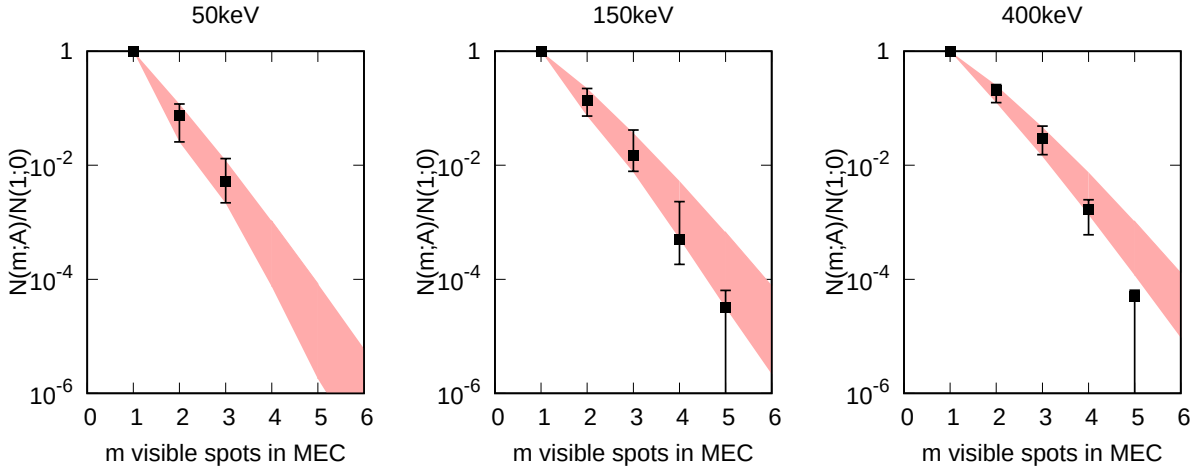

Fig. 3: The experimentally observed count, $N(m;A)$, for the m-tuples of spots which may be contained in a minimum enclosing circle (MEC) with diameter less than or equal to $d = 8nm$ (see text). Error bars denote counts of spots with intensities over different critical thresholds, with significance levels $\alpha = 0.15$ (higher value of error bar) to $\alpha = 0.001$, with the symbol at significance level $\alpha = 0.025$. The shaded region indicates a best fit for this observed count, assuming that individual cascades are independently generated. Again the upper and lower bounds correspond to intensity threshold significance levels of $\alpha = 0.15$ and $\alpha = 0.001$.

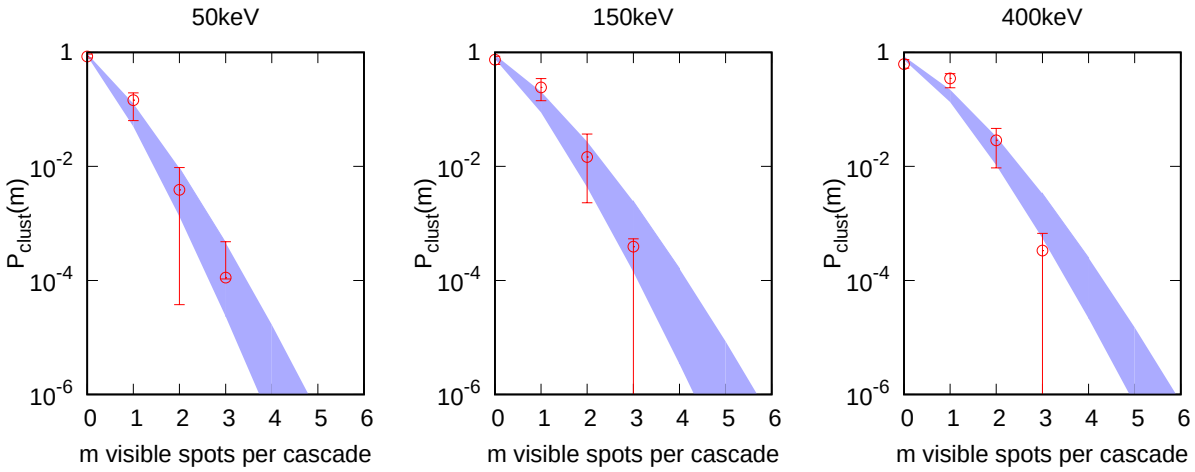

Fig. 4: The main result of this letter, the fitted distribution for the number of visible spots generated in individual primary damage cascades. Error bars denote counts of spots with intensities over different critical thresholds, with significance levels $\alpha = 0.15$ (higher value of error bar) to $\alpha = 0.001$, with the symbol at significance level $\alpha = 0.025$. Only the assumption of independent (non-overlapping) individual cascades is used for this fitting. The shaded region indicates a possible alternative fit (using the same threshold intensities for sampling the spots), with the additional assumption that the number of radiation-induced defect clusters produced in each cascade is Poisson distributed.

per MEC, ie $N(m;A)$, gives the shaded region in figure 4. This appears to be a good approximation for the best fit we were able to produce. We should stress that coincidence of these results should not imply causality - we have not proved here that visible defects *are* produced independently within individual cascades, only that the experimental evidence we have gathered is not inconsistent with this model.

Our analysis here is two-dimensional, based on the expected count of spots in a circular area. The three-dimensional nature of the cascade damage becomes relevant if there is a chance that the 'shadowing' of spots produced in a single cascade affects the answer - then we should misinterpret two separated defect clusters as one because they are aligned. Our conclusion in fig 4 is that there are 10x more cascades with one visible spot than with two well-separated visible spots in the plane. Therefore we can assume that the number of cascades with shadowed, well-separated, visible spots is lower than 10% of the single spot cascades. Shadowing will therefore not significantly affect our answer.

We conclude that in these *in situ* ion irradiations, the

incident ions initiate cascades, and in the heat spike phase nanoscale dislocation loops can be generated. While most cascades do not produce any visible defects, some produce loops large enough to be seen as spots in the TEM ($\gtrsim 2$ nm in our imaging conditions). There is no evidence for subsequent growth at cryogenic temperatures and very low fluence. In this paper we have shown that where large loops are generated, they do not only appear as isolated singletons, but can appear as pairs or triplets.

This work proves that rare events- the simultaneous production of multiple large loops within a single cascade- can not only be observed, but are likely to be important, providing stable nucleation sites for subsequent microstructural evolution in irradiated materials.

Acknowledgements. – The authors would like to thank Jack Haley, Oxford University, for many helpful discussions about the presentation of size-frequency histograms.

This work has been carried out within the framework of the EUROfusion Consortium and has received funding from the Euratom research and training programme 2014-2018 under grant agreement No. 633053, and was part-funded by the Research Councils UK Energy Programme [grant number EP/P012450/1]. The views and opinions expressed herein do not necessarily reflect those of the European Commission.

The experiments of in situ ion irradiations at liquid helium temperature were carried out at Argonne National Laboratory, using the IVEM-Tandem Facility. We thank to Dr Marquis Kirk, Pete Baldo and Edward Ryan for their help with the irradiations. This work was supported by a U.S. Department of Energy Facility funded by the DOE Office of Nuclear Energy, operated under Contract No. DE-AC02-06CH11357 by U. Chicago Argonne, LLC.

REFERENCES

[1] M.J. Norgett, M.T. Robinson, and I.M. Torrens. A proposed method of calculating displacement dose rates. *Nuclear Engineering and Design*, 33(1):50 – 54, 1975.

[2] R.E. Stoller. 1.11 - primary radiation damage formation. In Rudy J.M. Konings, editor, *Comprehensive Nuclear Materials*, pages 293 – 332. Elsevier, Oxford, 2012.

[3] M.A. Kirk, X. Yi, and M.L. Jenkins. Characterization of irradiation defect structures and densities by transmission electron microscopy. *Journal of Materials Research*, 30(9):1195–1201, 2015.

[4] A.A. Semenov and C.H. Woo. Stochastic fluctuations and microstructural evolution during irradiation by neutrons and heavy ions. *Journal of Nuclear Materials*, 205:74 – 83, 1993.

[5] C.H. Woo. Beyond the mean-field formulation of the production bias model. *Journal of Computer-Aided Materials Design*, 6(2):247–275, May 1999.

[6] A.A. Semenov and C.H. Woo. Stochastic effects on dislocation structure development under cascade-damage irradiation. *Applied Physics A*, 67(2):193–207, Aug 1998.

[7] A.A. Semenov, C.H. Woo, and E.A. Koptelov. Stochastic void coarsening. *Applied Physics A*, 73(3):335–340, Sep 2001.

[8] A. E. Sand, S. L. Dudarev, and K. Nordlund. High-energy collision cascades in tungsten: Dislocation loops structure and clustering scaling laws. *EPL (Europhysics Letters)*, 103(4):46003, 2013.

[9] D.R. Mason, X. Yi, M.A. Kirk, and S.L. Dudarev. Elastic trapping of dislocation loops in cascades in ion-irradiated tungsten foils. *J. Phys.: Condens. Matter*, 26:375701, 2014.

[10] X. Yi, A. E. Sand, D. R. Mason, M. A. Kirk, S. G. Roberts, K. Nordlund, and S. L. Dudarev. Direct observation of size scaling and elastic interaction between nano-scale defects in collision cascades. *EPL (Europhysics Letters)*, 110(3):36001, 2015.

[11] D.R. Mason, A.E. Sand, X. Yi, and S.L. Dudarev. Direct observation of the spatial distribution of primary cascade damage in tungsten. *Acta Materialia*, 144:905–917, 2018.

[12] A. E. Sand, D. R. Mason, A. De Backer, X. Yi, S. L. Dudarev, and K. Nordlund. Cascade fragmentation: deviation from power law in primary radiation damage. *Materials Research Letters*, 5(5):357–363, 2017.

[13] T.D. Swinburne, P.-W. Ma, and S.L. Dudarev. Low temperature diffusivity of self-interstitial defects in tungsten. *New Journal of Physics*, 19(7):073024, 2017.

[14] X. Yi, M.L. Jenkins, M. Briceno, S.G. Roberts, Z. Zhou, and M.A. Kirk. In situ study of self-ion irradiation damage in W and W-5Re at 500C. *Phil. Mag.*, 93(14):1715–1738, 2013.

[15] A. Prokhodtseva, B. Décamps, and R. Schäublin. Comparison between bulk and thin foil ion irradiation of ultra high purity Fe. *J Nucl Mater.*, 442:S786–S789, 2013.

[16] J.F. Ziegler, J.P. Biersack, and U. Littmark. *The stopping and range of ions in solids*. Pergamon, 1982.

[17] C. Liu, L. He, Y. Zhai, B. Tyburska-P uschel, P.M. Voyles, K. Sridharan, D. Morgan, and I. Szlufarska. Evolution of small defect clusters in ion-irradiated 3C-SiC: Combined cluster dynamics modeling and experimental study. *Acta Materialia*, 125:377 – 389, 2017.

[18] M.L. Jenkins and M.A. Kirk. *Characterization of Radiation Damage by Transmission Electron Microscopy*. Series in Microscopy in Materials Science. IOP, Bristol, 2001.

[19] R. Alexander, M.-C. Marinica, L. Proville, F. Willaime, K. Arakawa, M. R. Gilbert, and S. L. Dudarev. Ab initio scaling laws for the formation energy of nanosized interstitial defect clusters in iron, tungsten, and vanadium. *Phys. Rev. B*, 94:024103, Jul 2016.

[20] Jan Fikar, Robin Schublin, Daniel R. Mason, and Duc Nguyen-Manh. Nano-sized prismatic vacancy dislocation loops and vacancy clusters in tungsten. *Nuclear Materials and Energy*, 16:60 – 65, 2018.

[21] J. Fikar and R. Gröger. Interactions of prismatic dislocation loops with free surfaces in thin foils of body-centered cubic iron. *Acta Materialia*, 99:392 – 401, 2015.

[22] J. Fikar, R. Gröger, and R. Schäublin. Interaction of irradiation-induced prismatic dislocation loops with free surfaces in tungsten. *Nuclear Instruments and Methods in Physics Research Section B:*, 393:186 – 189, 2017.

[23] S.L. Dudarev and A.P. Sutton. Elastic interactions between nano-scale defects in irradiated materials. *Acta Materialia*, 125:425 – 430, 2017.